

EVALUATION OF BALLAST BEHAVIOR UNDER DIFFERENT TIE SUPPORT CONDITIONS USING DISCRETE ELEMENT MODELING

Wenting Hou¹

Ph.D. Student, Graduate Research Assistant

Tel: (217) 550-5686; Email: whou3@illinois.edu

Bin Feng¹

Ph.D. Student, Graduate Research Assistant

Tel: (217) 721-4381; Email: binfeng2@illinois.edu

Wei Li²

Ph.D. Student, Graduate Research Assistant

Tel: (217) 305-0023; Email: weili15@illinois.edu

Erol Tutumluer¹

Ph.D., Professor (Corresponding Author)

Paul F. Kent Endowed Faculty Scholar

Tel: (217) 333-8637; Email: tutumlue@illinois.edu

¹Department of Civil and Environmental Engineering
University of Illinois at Urbana-Champaign
205 North Mathews, Urbana, Illinois 61801

²Zhejiang University, Hangzhou, China

Word Count: 4,639 words + 1 Tables (1*250) + 8 Figures (8*250) = 6,889

TRR Paper No: 18-04833

Submission Date: March 15, 2018

ABSTRACT

This paper presents findings of a railroad ballast study using the Discrete Element Method (DEM) focused on mesoscale performance modeling of ballast layer under different tie support conditions. The simulation assembles ballast gradation that met the requirements of both AREMA No. 3 and No. 4A specifications with polyhedral particle shapes created similar to the field collected ballast samples. A full-track model was generated as a basic model, upon which five different support conditions were studied in the DEM simulation. Static rail seat loads of 10-kips were applied until the DEM model became stable. The pressure distribution along tie-ballast interface predicted by DEM simulations was in good agreement with previously published results backcalculated from laboratory testing. Static rail seat loads of 20 kips were then applied in the calibrated DEM model to evaluate in-track performance. Results from the validated full-track DEM simulations indicated that only a small portion of ballast particles participated in load distribution under static loading. Particles on the shoulders and particles in the areas with poor support conditions often experience none or very low contact forces. Load transfer mechanisms investigated through a contact force network varied greatly among different support conditions; lack of rail seat support, full support, and lack of center support had wider force distribution angles than the high center binding and severe center binding conditions. The severe center binding scenario was found to be the most critical support condition in terms of causing the highest tie-ballast contact pressure exceeding 30% the AREMA allowable pressure.

Key Words: Ballast, Tie, Support condition, Discrete Element Modeling (DEM), Normal stress distribution, Contact forces

INTRODUCTION

In U.S., most railway corridors are constructed as ballasted track. Ballasted track consists of two major parts, namely, superstructure and substructure. Superstructure includes rail, fastening system and tie; while substructure includes ballast, subballast, and subgrade. Ballast is an essential layer of railroad track substructure which provides load distribution as well as drainage. Ballast layer under repeated train moving loads undergoes shakedown and permanent deformation, which eventually lead to ballast degradation and track settlement. As indicated, the excessive dynamic or impact wheel loading is often the primary cause for ballast related track geometry deterioration (1, 2, 3). Therefore, it is important to better understand deterioration mechanisms of the particulate nature ballast behavior and the effects of its degradation modes on track condition assessment.

Discrete Element Method (DEM) has been proven as an effective method to simulate ballast layer deformation behavior under repeated train loading (4, 5, 6). Previous research studies on the DEM simulations of ballast behavior has focused on the particulate nature of ballast, for example, ballast particle size or gradation (5), ballast particle shape (7), degraded ballast (8), and geogrid reinforced ballast (9), and often studied ballast behavior from specific laboratory tests (10). Most of the studies listed above only considered full support interface between ballast and tie, which is certainly not representing the true individual particle point contact in-track support condition. McHenry et al. (11) quantitatively characterized ballast-tie interface pressure distribution in both laboratory testing and in-track testing using matrix-based tactile surface sensors. Results confirmed the variability of support conditions (load distribution) considering contact area as well as peak pressure. In addition, they also found that the location of measured peak pressures disagreed with the pressure distribution recommended in the AREMA Manual for Railway Engineering (12).

In the past, very few studies concentrated on ballast support conditions. Kaewunruen and Remennikov (13) investigated the influence of three types of ballast support conditions to concrete tie flexural performance by using finite element modeling, including half side support, symmetric support, and non-symmetric support conditions. Results indicated that the bending moments were affected significantly by the uneven ballast stiffness distribution. It was found that the nominal bending moment at mid-span could be eight times larger than the standard design moment at the most critical support condition. Gao et al. (14) recently introduced a ballast support condition backcalculator, which was used to quantify ballast pressure distributions under ties. In their study, strain gauges were installed on concrete ties to measure bending moments. Together with the measured rail seat loads, the ballast support condition backcalculator could estimate the in-track ballast support conditions beneath the tie. Figure 1 shows the laboratory experiment setup in their study. By varying the location of rubber pads underneath the crosstie, they simulated five different support conditions, including full support, lack of rail seat support, high center binding, lack of center support, and severe center binding.

Note that no previous literature can be found to focus on the ballast mesoscale behavior and investigate ballast particle contact force network, such as all normal and shear forces

Hou, Feng, Li, and Tutumluer

between two contacting particles within the ballast layer, under different ballast support conditions. Accordingly, this paper intends to fill this gap in our understanding by conducting DEM simulations of particulate nature ballast behavior under loading of strain gauge instrumented concrete ties with known support conditions in the laboratory.

OBJECTIVE AND SCOPE

The main objective of this paper is to investigate ballast-tie interaction under different tie support conditions and to better understand the stress distribution in ballast layer. The ultimate goal is to determine the most critical tie support scenarios leading to tie failures and track geometry deterioration and accordingly, provide guidance to railway maintenance and rehabilitation activities to ensure better performance of ballasted track. To achieve these inter-connected objectives, DEM modeling has been adopted in the scope to simulate the particulate nature ballast layer behavior under loading for five different support conditions. The five different support conditions were chosen based on a previous laboratory study conducted by Gao et al. (14) and are related to recorded field track conditions. The use of the same support conditions in DEM modeling allows comparing the predictions with the results from experiments, which essentially provides a methodology to calibrate the DEM model parameters. Next, the validated DEM model is utilized to produce more detailed mesoscale analyses of the ballast layer at current in-track loading level of 20 kips (315k car approximately) under different support conditions, such as force chain and stress distribution.

DEM SIMULATIONS OF DIFFERENT TIE SUPPORT CONDITIONS

Ballast Material Properties

In this study, polyhedral particles were employed to represent realistic shapes of ballast particles in the DEM simulations. A polyhedral 3D DEM code, BLOKS3D (15, 16), was used for the DEM simulations. The key particle morphological indices such as the Flat and Elongated (F&E) ratio and Angularity Index (in degrees) of field collected ballast particles were determined using the Enhanced University of Illinois Aggregate Image Analyzer (E-UIAIA) (17). Figure 2 shows these imaging based particle shape indices obtained by E-UIAIA. The gradation of ballast material adequately met both No. 3 and No. 4A gradations of American Railway Engineering and Maintenance-of-Way Association (AREMA). Table 1 lists the percent passing sieve sizes of the granite type ballast material used as the gradation input for the DEM simulations. The polyhedral particles were generated by BLOKS3D automatically based on the inputs of gradation and the shape properties quantified by E-UIAIA.

Simulation Approach

A full-track model was generated in BLOKS3D with the layout shown in Figure 3. A simple concrete tie representation with dimensions of $10\frac{3}{8} \times 9\frac{5}{8} \times 102$ in. ($0.2635 \times 0.244 \times 2.59$ m) was placed on top of a 14-in. (0.36-m) thick ballast layer. Full width of the track was modeled with 11.8-in. (0.3-m) wide ballast shoulders and 2:1 shoulder slope. The length in the train moving

Hou, Feng, Li, and Tutumluer

direction was chosen as 24-in. (0.61-m), which is approximately one tie spacing. After the geometry of DEM simulation was determined, ballast particles were gravity dropped into the defined geometry. Around 11,000 particles were used in the simulation. Compaction of the ballast particles were accomplished by placing a non-deformable plate on top of the ballast layer and pushing downward until the density targeted in track was achieved. Once the basic ballast creation and compaction in DEM was done, the concrete tie was generated as a non-deformable master block in BLOKS3D and placed on top of the ballast layer. Note that since only a non-deformable master block is available in the code, the tie created is not able to bend as in reality, which may affect the tie-ballast pressure distribution to some extent. It was considered as acceptable in this study since the focus is the ballast layer performance, rather than crosstie bending flexural performance.

In the DEM simulation, some key model parameters were determined after trial and error and based on the previous knowledge from DEM simulations (4, 8, 10), such that the normal contact stiffness was adjusted to 20 MN/m; the shear contact stiffness was adjusted to 10 MN/m; global damping ratio was nil; contact damping ratio was adjusted to 0.40; and the surface friction angle related to the roughness of contacting aggregate particles was 31°.

Model Calibration with Laboratory Test Results

The purpose of model calibration is to determine the model parameters which produce the DEM simulation results that match with laboratory test results. The schematic profile view drawing of the five different support conditions simulated in the laboratory experimental setup are shown in Figure 4 (a) which illustrates: (1) full support, representing an idealized track, condition; (2) lack of rail seat support condition, representing the in-track condition caused by high impact wheel loads, as insufficient support under rail seats; 3) lack of center support condition, representing the idealized track condition right after tamping, which provides adequate support under the rail seats and decreased support on the center of the crosstie; (4) high center binding; and finally, (5) severe center binding support representing extreme cases where the track support migrates towards the center of the crosstie.

A total of five strain gauges were installed on the crosstie, with one at each rail seat, one at the center, and another located halfway between each rail seat and center as shown on top of the crosstie in Figure 4 (18). Rubber pads were used beneath the crosstie to simulate ballast support (19). Overall the bottom of the concrete crosstie was divided into six equally spaced sections. By varying the locations of rubber pads, five different support conditions were simulated. A static load of 10 kips (44.5 kN) was applied to each rail seat. The bending moments and two static rail seat loads were used as inputs in the backcalculator program to calculate the tie-ballast reaction force distribution (14).

To simulate the five different support conditions in laboratory testing, five full-track models were generated based on the basic DEM model. Figure 4 (b) shows the profile views of track models for different support conditions. For example, to create the severe center binding support condition, before placing the tie on top of ballast layer, more ballast particles were dropped only at the center of existing ballast layer and compacted to target density. After the full-track models were formed, two static rail seat loads of 10 kips (44.5 kN) each were applied

vertically until the ballast layer was stable under the external loading. The force exerted on each ballast particle was obtained from the DEM simulations. From the laboratory testing backcalculation results (14), the tie-ballast reaction force at each rubber pad (17-in./0.43-m) was consistent. To make a valid comparison, the external forces exerted on surface ballast particles at the six corresponding rubber pad locations were summed up separately to obtain tie-ballast reaction force distributions from the DEM simulations.

Figure 5 presents the tie-ballast reaction force distributions obtained from both the DEM simulations and the laboratory tests. For almost all support conditions simulated, the overall reaction force distribution trends as well as the magnitude in percentage from both the laboratory and DEM simulations were in good agreement. One inconsistent comparison was the full support condition (see Figure 5b), where the laboratory results showed that the reaction force was very low in the center section and more concentrated below the rail seat sections, rather than more concentrated in the left half of the cross-tie section from the DEM simulation. This can probably be due to the following: (1) the discrete nature of DEM simulation may cause abrupt and sharp corner/edge on the left half side of tie-ballast contact surface, which will lead to force concentration in the DEM simulation; (2) rubber pad used in laboratory testing simulated an ideal uniform support condition, while in DEM simulation the particles were generated randomly that do not guarantee symmetrical or uniform stiffness; (3) the concentrated force may cause ballast particle breakage in reality and thus re-distribute the forces evenly among particles, while in the current BLOKS3D code no particle breakage is considered and accordingly, force concentration would not dissipate; and finally, (4) under the external forces applied on two rail seats, edges and center of the tie will bend and lift up in the laboratory tests while the tie is non-deformable in the DEM simulations. Despite the inconsistent trends observed from full support condition, it can be noticed that the tie-ballast force at each observation point is still within a reasonable range. From Figure 5, it may be concluded that the DEM simulation results based on the current set of model parameters could reasonably match the laboratory test results. Therefore, the calibrated DEM model can be used to predict different in-track ballast support conditions.

RESULTS AND DISCUSSION

In this section, mesoscale stress tensor formulas are derived. The formulas are adequate to calculate stresses in particles with rotation. To better study the in-track ballast behavior under different tie support conditions, the field monitored rail seat load of 20 kips (89 kN) from the Northeast Corridor was applied as the static loading in the calibrated DEM model. The magnitude and distribution of particle vertical normal stress σ_{33} and particle contact force network were visualized and analyzed using the calibrated DEM model.

Calculation of Stress Tensor

In order to analyze mesoscale structure of a ballast layer under external loading, mathematical formulas are required to properly calculate the stress tensor for a single particle. Roul and Schineer (20) derived stress tensor formulas for particles without rotation as follows:

Hou, Feng, Li, and Tutumluer

$$\langle \sigma_{ij} \rangle = \frac{1}{V} \sum_{p=1}^n \sum_{c=1}^{c^p} x_j^c F_i^c \quad (1)$$

where

F^c = contact force acting at the point c;

x^c = corresponding branch vector from the center of the mass of the particle p to contact point c.

During discrete element modeling, relative rotation exists between polyhedral particles and creates inertia forces on the particle. In order to adjust Eq. (1) for polyhedral particles with rotation, assuming the angular velocity and angular acceleration for a polyhedral particle P are ω^P and $\dot{\omega}^P$, forces caused by particle rotation can be expressed in the form of:

$$R_{ij}^P = \omega_k^P \omega_j^P J_{ik}^P - \omega_k^P \dot{\omega}_k^P J_{ij}^P + \Phi_{jkl} \omega_l^P J_{ij}^P \quad (2)$$

where

$$J_{ij}^P = \oint \rho x_i r_j dV^P = \oint \rho r_i r_j dV^P;$$

Φ_{jkl} = permutation tensor.

Inserting Eq. (2) in Eq. (1), the stress tensor formula for dynamic conditions are obtained in Eq. (3). Sigma is used on R_{ij}^P to sum all forces caused by rotation on particle P.

$$\langle \sigma_{ij} \rangle = \frac{1}{V} \left(\sum_{p=1}^n \sum_{c=1}^{c^p} x_j^c F_i^c + \sum_{P=1}^n R_{ij}^P \right) \quad (3)$$

where

F^c and x^c are defined as the same as Eq. (1);

R^P = force acting on particle P caused by rotation (Figure 6).

Vertical Normal Stress σ_{33} Distribution

Using Eq. (3), the force distribution can be calculated as a 3×3 matrix indicating normal forces and shear forces in x, y, z directions obtained for every single particle. Indices 1, 2, 3 represent x, y, z directions, respectively. σ_{33} is the vertical normal stress in every ballast particle to react the external force applied on the crosstie. The magnitude and distribution of σ_{33} from the analysis can offer a better insight into to the ballast layer performance in mesoscale.

Vertical normal stress σ_{33} magnitudes and distributions for the DEM model with five different support conditions were computed next. The visualized results are presented in Figure 7. Darker color in the figure indicates higher vertical normal stresses whereas lighter color indicates none or low vertical normal stresses.

From the visualized results, clear differences exist in the vertical normal stress distributions among the different support conditions. In lack of rail seat support condition, few

Hou, Feng, Li, and Tutumluer

ballast particles under rail seat contribute to reacting the external force; high stress concentration was observed in the center area of tie and ballast layer. Such high stress level would probably lead to higher settlement in the center and eventually develop a gap between tie and ballast layer. On the contrary, a better vertical normal stress distribution appears throughout the ballast layer in full support condition; particles with high stresses are fewer than other four different support conditions. As for lack of center support condition, several ballast particle zones with high normal stress concentrations exist with depth directly under rail seats where ballast particles are prone to crushing. Center binding conditions usually create higher vertical normal stresses in the middle and little load spreading with depth. To be more specific, in the high center binding condition, particles close to the middle of the crosstie experience very high vertical normal stresses; a high stress concentration is not seen on either end of the ballast cross section. Furthermore, in severe center binding condition, high vertical normal stresses concentrate in the middle section of the ballast layer from top to bottom.

Besides the apparent differences, similarities are also observed among the presented five different support conditions. The ballast layer was constructed with about 11,000 particles in the DEM model, however, only a small portion of particles contribute to the reaction force. Particles on the shoulder and particles in the area with poor support condition often experience none or very low stresses under the external loading. Only few particles near the tie-ballast contact surface tend to experience extremely high vertical normal stresses under the external loading. Particles with such large stresses have high possibilities to break down into smaller particles. After breakage, such high stresses will transmit to other particles and lead to further breakage until a lower magnitude contact stress network than can be tolerated by ballast particle rigidity is maintained. Note that more particle breakage and degradation will occur with the growth of external loading cycles to contribute to an increasing Fouling Index (FI), as defined by Selig and Waters (*I*), in the ballast layer. Higher FI values will eventually impact drainage ability of the ballast layer and lead to faster ballast degradation and track deterioration. Among all the studied ballast support conditions, severe center binding seems to be the most critical scenario in terms of reaction force concentration and the ballast degradation potential.

Contact Force Network

Visualizing the contact force network among particles is an effective and widely used method to study the mesoscale structure of unbound granular materials (21, 22). One of the advantages of using contact force network is that ballast layer can be visualized through the width with no concern about ballast particles in the front obstructing the view of the ballast particles in the back. Contact force networks for the five different support conditions are visualized in Figure 8, where the line thickness and darkness are both indicative of the higher magnitude contact forces.

Figure 8 clearly indicates that the contact force networks match well with their actual support conditions. Darker and thicker lines concentrate in the areas with good support condition while lighter and thinner lines prevail in the areas with poor support condition. One exception is that the force network in full support condition, where the contact force network seems a little concentrated in the left half side of the crosstie rather than evenly distributed along the crosstie as expected. Possible reason is that the crosstie first contacts with some ballast particles on the

Hou, Feng, Li, and Tutumluer

left when the loads were applied. Even though the tie-ballast contact surface appears flat in the model, due to its discrete nature, ballast particles are not easy to be distributed evenly across the contact surface. Similar findings were observed by McHenry et al. (11) that the pressure distribution between ballast and tie measured in laboratory at full support condition was not uniform but with point load concentrations. Force diffusion is obvious in lack of rail seat support condition and lack of center support condition while it is not clear in high center binding condition and severe center binding condition. Force network results are in good agreement with the observations from the vertical normal stresses in the previous section; fewer dark network lines indicate more concentrated reaction force. Large magnitudes of the reaction force exist and transmit only in a few particles. Ballast shoulders and areas with poor support condition rarely have dark and thick lines. The poorer the support condition, the more the contact forces concentrate in the case of a limited number of ballast particles which may eventually lead to particle breakage. The maximum tie-ballast contact pressure was also recorded as 97, 70, 102, 77, and 114 psi, for support conditions from (a) to (e), respectively. As expected, the full support condition exhibits the smallest tie-ballast contact force. AREMA assumes an allowable ballast pressure under concrete crossties to be 85 psi (586 kPa) (12). Only the full support and high center binding conditions satisfy this requirement for the in-track load level. Note that the maximum tie-ballast contact pressure under lack of rail seat support and lack of center support conditions are similar in magnitude. Finally, the most critical condition is severe center binding, which exceeds the allowable contact pressure by 30%.

CONCLUSIONS

Five realistic full-track ballast simulation models, each representing one unique support condition commonly found in track, were developed and analyzed using the Discrete Element Method (DEM) with the consideration of realistic 3D polyhedral ballast particles. The DEM models were based on the available test data obtained from previously conducted laboratory testing conditions. For the model calibration effort, the DEM simulation results of the tie-ballast contact force distributions matched well in both magnitude and overall trend with those backcalculated results obtained from the laboratory tests, which had used strain gauges instrumented on the tested crosstie. The calibrated DEM model was then used to predict in-track performance under 20-kip rail seat loads. Stress tensor formulas were derived for calculating ballast particle stresses with relative rotation. Vertical normal stress magnitudes and distributions within ballast layer were successfully visualized. In addition, contact force networks showing the force chains in the ballast layer were successfully visualized for the different tie support conditions. The following conclusions can be drawn from this study:

1. Only a portion of ballast particles participated in load distribution when external forces were applied;
2. Good support condition indicates better force distribution throughout the ballast layer in terms of lower magnitude normal stresses and more evenly distributed force network;

Hou, Feng, Li, and Tutumluer

3. Poor support condition leads to higher stress concentrations on a few particles, which would increase the breakage possibility and ballast fouling tendencies, leading to faster track deterioration.

4. DEM simulation results show high normal stresses on ballast layer under loading. While no particle breakage was considered in the simulation, in reality such high normal stresses can lead to particle breakage.

5. DEM simulation results show that different support conditions influence ballast contact force distribution greatly. Lack of rail seat support, full support, and lack of center support have wider force distribution angles than high center binding and severe center binding conditions.

6. The severe center binding scenario seems to be the most critical support condition in terms of generating non-uniform contact force distributions and highest tie-ballast contact forces among the studied five support conditions that exceed the AREMA allowable pressure of 85 psi by 30%.

ACKNOWLEDGEMENTS

The support for this study was partly provided by the Amtrak Concrete Tie and Track Structure Improvement project undertaken in the Rail Transportation and Engineering Center (RailTEC) at the University of Illinois at Urbana-Champaign (UIUC). The authors would like to acknowledge J. Riley Edwards and the project team members for their useful advice at different stages of this research. The contents of this paper reflect the views of the authors who are responsible for the facts and the accuracy of the data presented herein. This paper does not constitute a standard, specification, or regulation.

AUTHOR CONTRIBUTION STATEMENT

The authors confirm contributions to the paper as follows. Study conception and design: Wenting Hou, Erol Tutumluer; data collection: Wenting Hou, Bin Feng; analysis and interpretation of results: Wenting Hou, Bin Feng, Wei Li; draft manuscript preparation: Wenting Hou, Bin Feng, Wei Li, Erol Tutumluer. All authors reviewed the results and approved the final version of the manuscript.

REFERENCES

1. Selig, E. T., & Waters, J. M. (1994). Track geotechnology and substructure management. Thomas Telford.
2. Li, D., & Davis, D. (2005). Transition of railroad bridge approaches. *Journal of Geotechnical Engineering*, 131(11):1392-1398.
3. Mishra, D., Tutumluer, E., Stark, T. D., Hyslip, J. P., Chrismer, S. M., & Tomas, M. (2012). Investigation of differential movement at railroad bridge approaches through geotechnical instrumentation. *Journal of Zhejiang University SCIENCE A*, 13(11), 814-824.

Hou, Feng, Li, and Tutumluer

4. Tutumluer, E., Huang, H., Hashash, Y. M. A., & Ghaboussi, J. (2007). Discrete element modeling of railroad ballast settlement. In Proceedings of AREMA Conference, September.
5. Tutumluer, E., Huang, H., Hashash, Y. M. A., & Ghaboussi, J. (2009, September). AREMA gradations affecting ballast performance using discrete element modeling (DEM) approach. *In Proceedings of the AREMA 2009 Annual Conference, Chicago, Illinois, September*, pp. 20-23.
6. Tutumluer, E., Qian, Y., Hashash, Y. M. A., Ghaboussi, J., & Davis, D. D. (2011). Field validated discrete element model for railroad ballast. *In Proc., Annual Conference of the American Railway Engineering and Maintenance-of-Way Association*, pp. 18-21.
7. Lu, M., & McDowell, G. R. (2007). The importance of modelling ballast particle shape in the discrete element method. *Granular matter*, 9(1-2), 69.
8. Huang, H., & Tutumluer, E. (2011). Discrete element modeling for fouled railroad ballast. *Construction and Building Materials*, 25(8), pp. 3306-3312.
9. Ngo, N. T., Indraratna, B., & Rujikiatkamjorn, C. (2014). DEM simulation of the behavior of geogrid stabilized ballast fouled with coal. *Computers and Geotechnics*, 55, pp. 224-231.
10. Qian, Y., Lee, S., Tutumluer, E., Hashash, Y., Mishra, D., & Ghaboussi, J. (2013). Simulating ballast shear strength from large-scale triaxial tests: Discrete element method. *Transportation Research Record: Journal of the Transportation Research Board*, 2374, pp. 126-135.
11. McHenry, M. T., Brown, M., LoPresti, J., Rose, J., & Souleyrette, R. (2015). Use of Matrix-Based Tactile Surface Sensors to Assess Fine-Scale Ballast-Tie Interface Pressure Distribution in Railroad Track. *Transportation Research Record: Journal of the Transportation Research Board*, 2476, pp. 23-31.
12. In Manual for Railway Engineering, American Railway Engineering and Maintenance-of-Way Association, Lanham, MD, 2012.
13. Kaewnuen, S., & Remennikov, A. M. (2009). Influence of ballast conditions on flexural responses of railway concrete sleepers. *Concrete in Australia: Journal of Concrete Institute of Australia*, 35(4), pp. 57-62.
14. Gao, Z., Wolf, H. E., Dersch, M. S., Qian, Y., & Edwards, J. R. (2016). Field Measurements and Proposed Analysis of Concrete Crosstie Bending Moments. *In Proceedings of the American Railway Engineering and Maintenance of Way Association Annual Meeting*. Orlando, Florida.
15. Ghaboussi, J., & Barbosa, R. (1990). Three-dimensional discrete element method for granular materials. *International Journal for Numerical and Analytical Methods in Geomechanics*, 14(7), pp. 451-472.
16. Zhao, D., Nezami, E. G., Hashash, Y. M., & Ghaboussi, J. (2006). Three-dimensional discrete element simulation for granular materials. *Engineering Computations*, 23(7), pp. 749-770.
17. Moaveni, M., Wang, S., Hart, J.M., Tutumluer, E., & N. Ahuja (2013). "Aggregate Size and Shape Evaluation Using Segmentation Techniques and Aggregate Image Processing Algorithms," *Transportation Research Record 2335, Journal of the Transportation Research Board, National Research Council, Washington, D.C.*, pp. 50-59.

Hou, Feng, Li, and Tutumluer

18. Wolf, H. E. (2015). Flexural behavior of prestressed concrete mono block crossties (Doctoral dissertation). University of Illinois at Urbana-Champaign, Champaign, Illinois.
19. César Bastos, J. (2016). Analysis of the performance and failure of railroad concrete crossties with various track support conditions (Doctoral dissertation).
20. Roul, P. & A. Schinner (2010). "Simulation study on micro and macro mechanical behavior of sand piles." *Powder Technology* 204(1), pp. 113-123.
21. O'Sullivan, C., et al. (2008). "Discrete Element Analysis of the Response of Granular Materials during Cyclic Loading." *Soils and Foundations* 48(4), pp. 511-530.
22. Sazzad, M. M. & K. Suzuki (2010). "Micromechanical behavior of granular materials with inherent anisotropy under cyclic loading using 2D DEM." *Granular Matter* 12(6), pp. 597-605.

LIST OF TABLES**TABLE 1 Gradation of the Ballast Material Used in DEM Simulations****LIST OF FIGURES**

FIGURE 1 Laboratory experiment setup for simulating different support conditions (14).

FIGURE 2 Imaging based 3D ballast particle shape properties quantified by E-UIAIA.

FIGURE 3 Basic one-tie ballast layer geometry established in DEM simulation.

FIGURE 4 (a) Schematic profile view drawings of the five different support conditions in laboratory testing (14) (b) Profile views of five different support conditions in DEM simulations.

FIGURE 5 Comparisons of tie-ballast reaction forces backcalculated from laboratory testing to those predicted from DEM simulations (a) Lack of rail seat support (b) Full support (c) Lack of center support (d) High center binding (e) Severe center binding.

FIGURE 6 Schematic of random particle P.

FIGURE 7 Vertical normal stress distributions of the ballast layers with five different support conditions (a) Lack of rail seat support (b) Full support (c) Lack of center support (d) High center binding (e) Severe center binding.

FIGURE 8 Contact force networks of the ballast layers with five different support conditions (a) Lack of rail seat support (b) Full support (c) Lack of center support (d) High center binding (e) Severe center binding.

TABLE 1 Gradation of the Ballast Material Used in DEM Simulations

Sieve Size		Percent Passing (%)
2 ½"	63.5 mm	100
2"	50.8 mm	95
1 ½"	38.1 mm	65
1"	25.4 mm	10
½"	12.7 mm	0

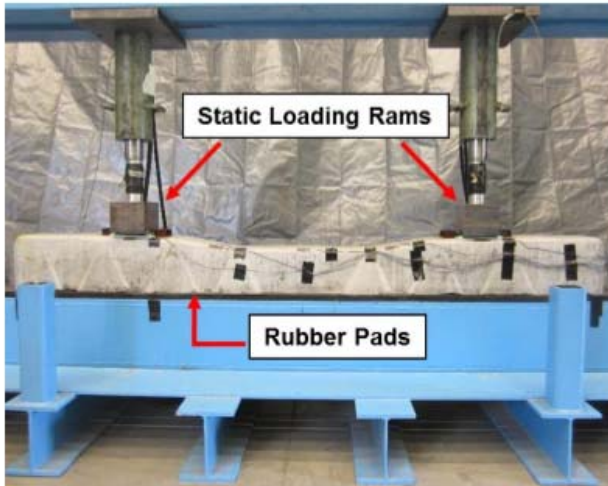


FIGURE 1 Laboratory experiment setup for simulating different support conditions (14).

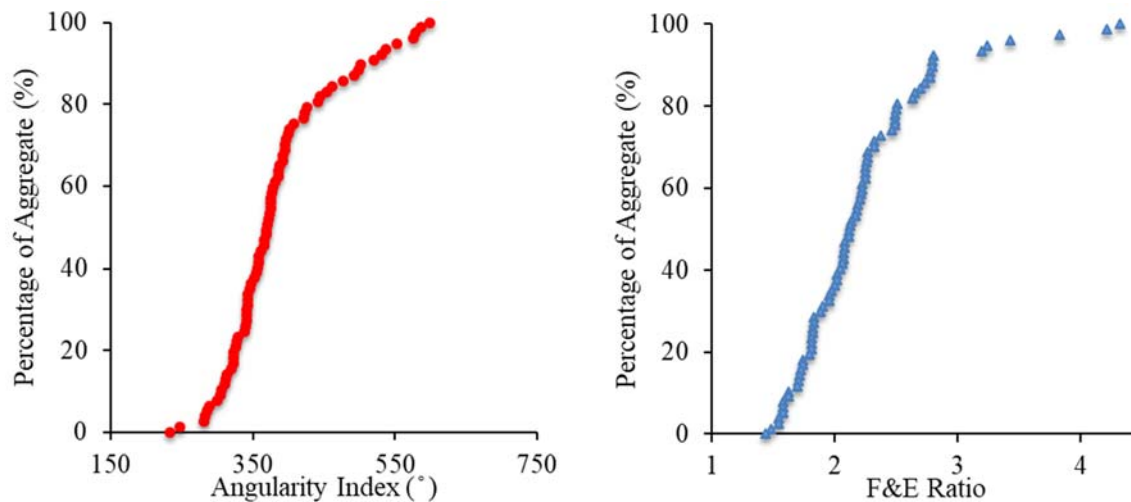


FIGURE 2 Imaging based 3D ballast particle shape properties quantified by E-UIAIA.

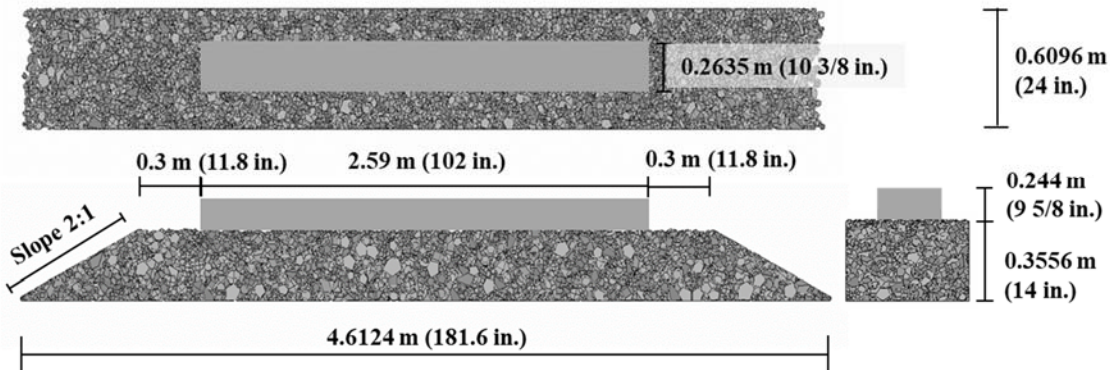


FIGURE 3 Basic one-tie ballast layer geometry established in DEM simulation.

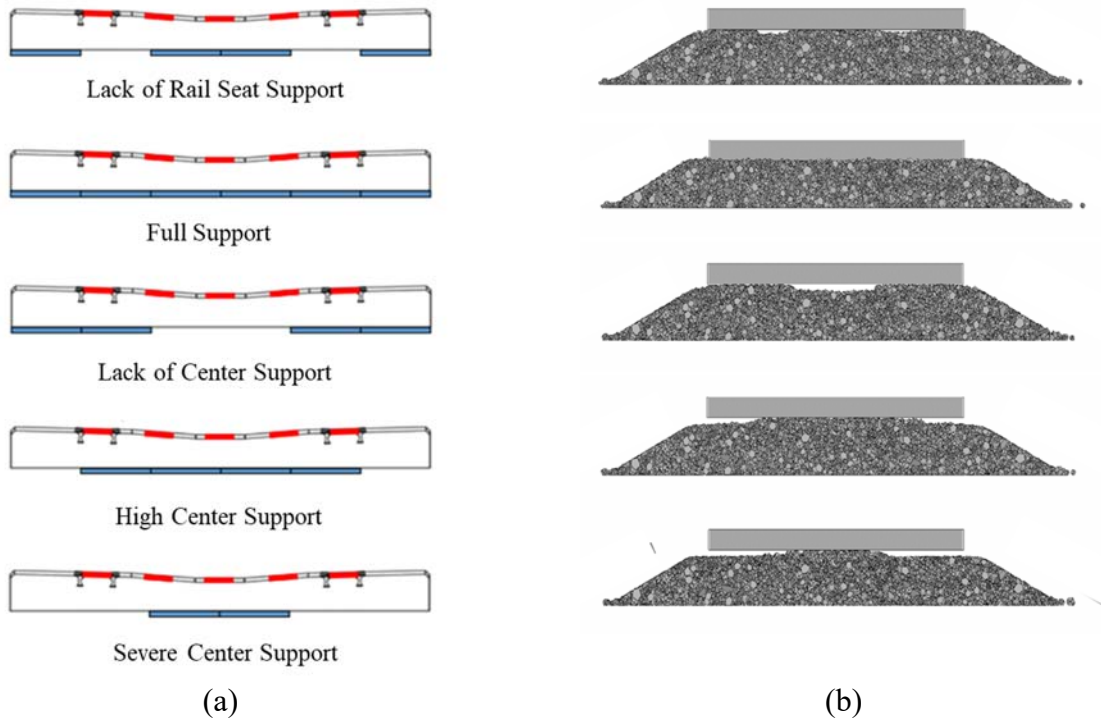


FIGURE 4 (a) Schematic profile view drawings of the five different support conditions in laboratory testing (14) (b) Profile views of five different support conditions in DEM simulations.

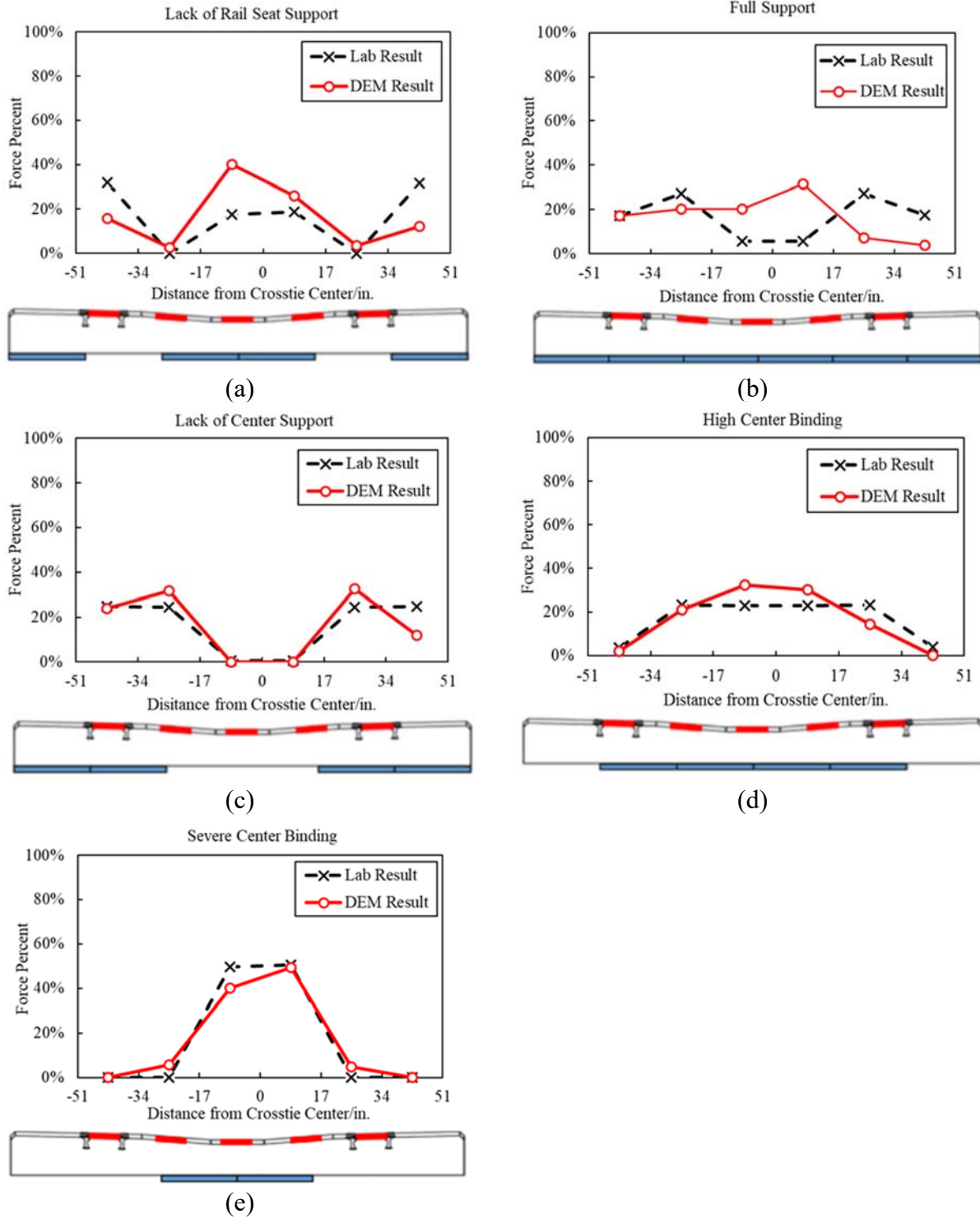


FIGURE 5 Comparisons of tie-ballast reaction forces backcalculated from laboratory testing to those predicted from DEM simulations (a) Lack of rail seat support (b) Full support (c) Lack of center support (d) High center binding (e) Severe center binding.

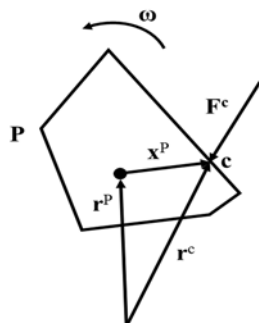


FIGURE 6 Schematic of random particle P.

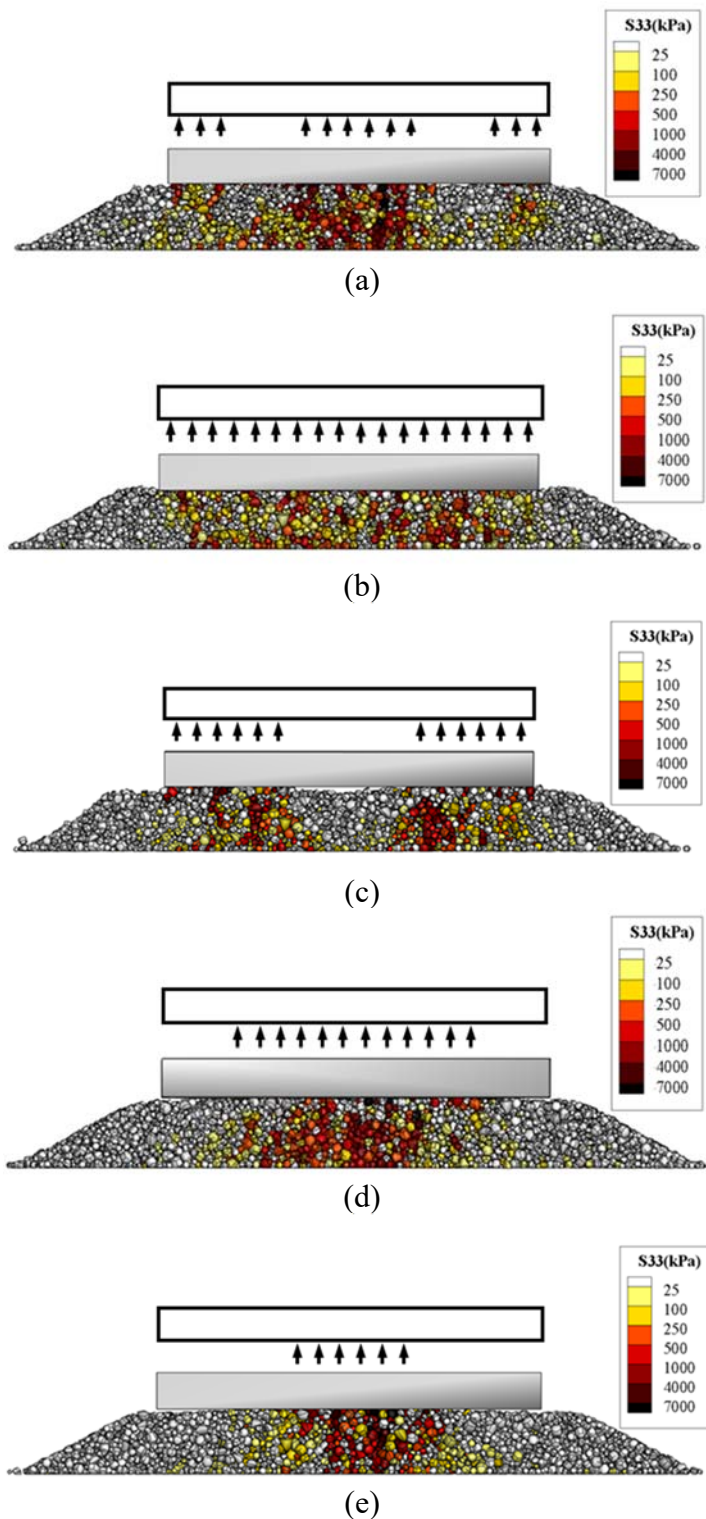


FIGURE 7 Vertical normal stress distributions of the ballast layers with five different support conditions (a) Lack of rail seat support (b) Full support (c) Lack of center support (d) High center binding (e) Severe center binding.

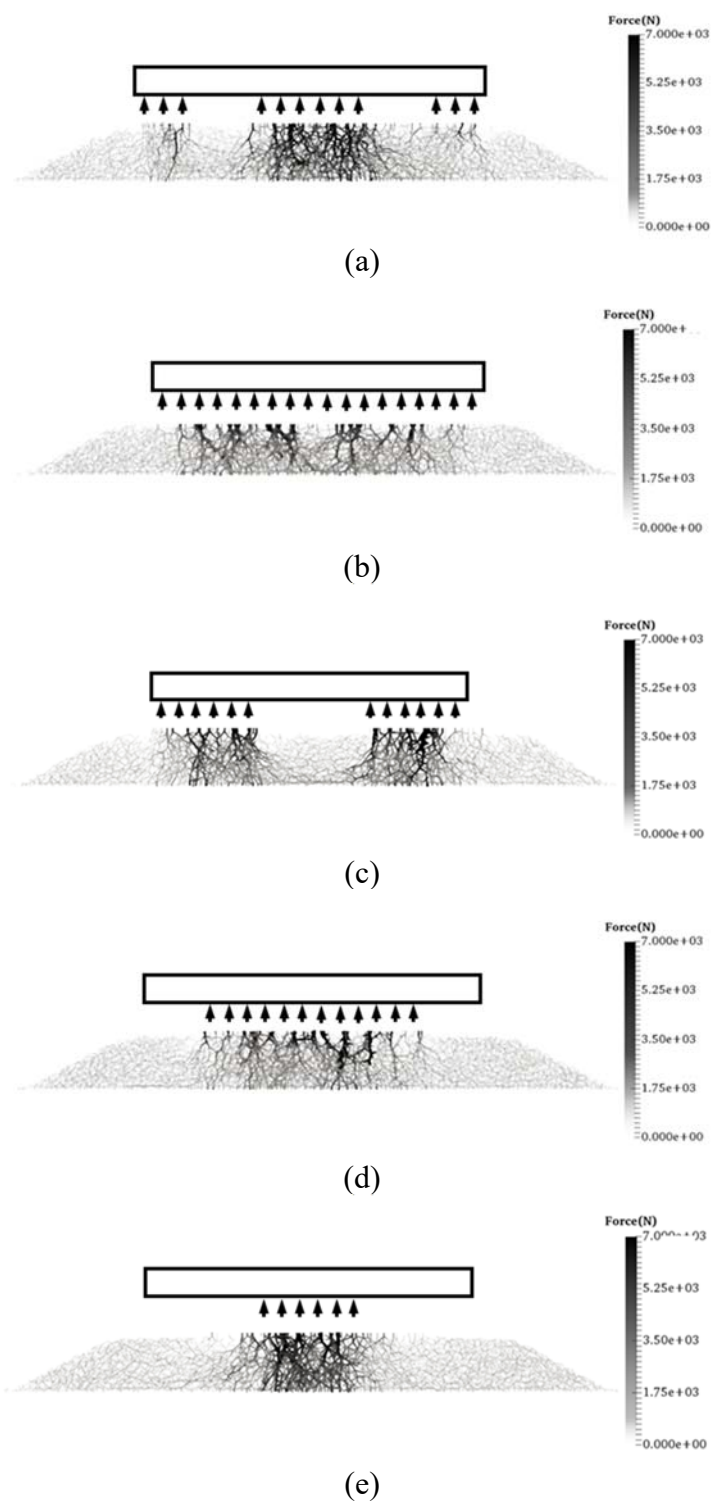


FIGURE 8 Contact force networks of the ballast layers with five different support conditions (a) Lack of rail seat support (b) Full support (c) Lack of center support (d) High center binding (e) Severe center binding.